Modelling of R/C members accounting for shear failure localisation: Finite element model and verification

Dimitrios K. Zimos[a], Panagiotis E. Mergos[a] and Andreas J. Kappos[a,b]

[a] *Research Centre for Civil Engineering Structures, Civil Engineering Department, City, University of London, London, EC1V 0HB, United Kingdom*
[b] *Civil Engineering Department, Aristotle University of Thessaloniki, Thessaloniki, GR 54124*

SUMMARY

Reinforced concrete (R/C) frame buildings designed according to older seismic codes represent a large part of the existing building stock worldwide. Their structural elements are often vulnerable to shear or flexure-shear failure, which can eventually lead to loss of axial load resistance of vertical elements and initiate vertical progressive collapse of a building. In this study, a computationally efficient member-type finite element model for the hysteretic response of shear critical R/C frame elements up to the onset of axial failure is presented; it accounts for shear-flexure interaction and considers, for the first time, the localisation of shear strains, after the onset of shear failure, in a critical length defined by the diagonal failure plane. Its predictive capabilities are verified against experimental results of column and frame specimens and are shown to be accurate not only in terms of total response, but also with regard to individual deformation components. The accuracy, versatility and simplicity of this finite element model make it a valuable tool in seismic analysis of complex R/C buildings with shear deficient structural elements.

Keywords: Reinforced concrete structures; Substandard members; Finite element model; Shear failure localisation; Post-peak response; Axial failure

1. INTRODUCTION

The post-peak response of shear and flexure-shear critical R/C elements has to be appropriately captured, in order to correctly assess the degrading behaviour of sub-standard structures, especially when it comes to predicting the initiation and cascade of progressive collapse [1]. In addition, for analytical models to be realistic and reliable, they should be able to reliably predict the location and extent of shear damage, as measured by shear deformations, after the onset of shear failure, duly accounting for localisation effects.

Localisation is a ubiquitous and multifaceted phenomenon in structural engineering. Simple, yet well-known examples are the “necking” in tensile loading of steel and other metal materials as well as the concentration of damage at a specific region of a concrete specimen under compressive loads or the tensile crack region under tension [2]. In the case of shear deficient R/C elements, as presented and discussed extensively elsewhere [1], localisation arises from the formation of a diagonal failure plane, wherein shear deformations are concentrated after the onset of shear failure, namely shear failure localisation.

Initial efforts to model the seismic response of R/C elements were focused on flexural response and used concentrated inelasticity models (e.g. [3]) assuming that inelasticity is lumped in rotational springs at the member ends. In these models, shear deformations can be taken into account either by modifying the hysteretic rules of the rotational springs (e.g. [4]) or by adding translational shear springs (e.g. [5]). There have been several lumped inelasticity models for cyclic lateral behaviour of shear-deficient R/C elements that take into account shear deformations and the effect of shear-flexure interaction (e.g. [6]–[11]). Some of them also extend into the post-peak domain of the response, even predicting the onset of axial failure of an element (e.g. [9]–[11]), which is a critical point in assessing the behaviour of an existing structure, as it signals the initiation of vertical load redistribution and possibly progressive collapse. Lumped inelasticity models, albeit computationally efficient, are bound by limitations regarding their ability to predict inelastic response. More particularly, they cannot capture the gradual

spread of inelasticity, they rely on assumptions regarding the moment distribution of structural elements and they cannot provide information regarding the actual distribution of deformations and damage along the structural elements.

To tackle these limitations, 'distributed' inelasticity models (e.g. [12]–[30]), which either capture the inward penetration of inelasticity from the ends of an element (plastification zones of variable length), or define inelasticity at a sectional level. Distributed inelasticity models can be divided into two main categories: displacement-based (e.g. [15]) and force-based (e.g. [16]). The latter do not rely on assumptions regarding the displacement and curvature fields and, therefore, are considered more effective in modelling the inelastic response of structural elements. The first distributed inelasticity elements, both force and displacement-based, focused solely on flexural response (e.g. [15], [16]). These models are generally able to capture adequately the response of flexure-dominated R/C elements. In addition, a significant number of distributed inelasticity models have been developed to account for shear flexibility and shear-flexure interaction effects (e.g. [17]–[30]). These elements consider interaction of flexural and shear deformation deformations at a sectional level either by using mechanical models or by adopting phenomenological $V - \gamma$ (shear force – shear strain) laws (e.g. [14], [30]). A limited number of these models (e.g. [24], [30]) have also been extended to address response after the onset of shear failure.

Distributed inelasticity models have been found to suffer from numerical localisation issues in the post-peak range of the response, i.e. in the softening regime [2]. Numerical localisation should not be confused with the physical localisation occurring in structural elements during their softening response as described above; it is actually an inherent flaw of these finite elements, due to their numerical formulation, that leads to a steady increase of local deformations at the section where failure initiates as the number of integration points and/or mesh refinement increases, at the same value of the total displacement demand. This happens because, when softening is developed, inelasticity is concentrated solely at the most stressed integration point (controlling section) and the associated integration length. Therefore, the global and local predictions of distributed inelasticity elements depend on the applied finite element mesh or adopted numerical integration scheme (number and location of integration points) and therefore are not objective. To restore objectivity, several researchers have proposed regularisation techniques to overcome the problem of numerical localisation in the case of softening flexural response (e.g. [2], [31], [32]). These techniques aim at providing objective solutions that are realistic and physically meaningful in terms of the magnitude and spread of local deformations after the onset of flexural failure. Nonetheless, to the best of the authors' knowledge, no previous study addressed regularisation of post-peak response in the case of shear failure.

A computationally efficient member-type model for the full-range response of shear critical R/C members is put forward in this paper. The proposed formulation is based on an existing, flexibility-based (force-based) distributed inelasticity three-component finite element (flexure, shear and bond slip); the model captures the gradual spread of inelastic flexural and shear deformations as well as shear-flexure interaction at the locations of the plastic hinges up to the onset of shear failure [14]. The present study expands the afore-described model to capture the response after initiation of shear failure and up to the onset of axial failure of R/C columns. The novelty of the proposed approach lies in the consideration of the localisation of shear strains in the critical shear length L_{cr}, as determined in a recently submitted companion paper [1]; inside L_{cr}, the finite element model adopts the local hysteretic shear model calibrated and described in detail in [1]. Following this approach, the proposed formulation provides an objective and physically meaningful and consistent representation of the magnitude and distribution of shear deformations after the onset of shear failure, while avoiding numerical localisation issues related to distributed inelasticity elements.

In the remainder of the paper, the formulation of the proposed finite element is presented in detail. Furthermore, the predictions of the finite element are verified against quasi-static cyclic tests of shear and flexure-shear critical R/C column specimens as well as an R/C frame specimen tested on the shake-table. In addition to predicting the total response of these elements, the response with regard to separate

deformation components (i.e. flexure, shear and anchorage slip) is also compared wherever possible. The latter adds more value to the credibility of the proposed model.

2. FINITE ELEMENT MODEL DESCRIPTION

The phenomenological, force-based, distributed inelasticity beam-column model by Mergos & Kappos [14] is used as the basis to model the post-peak response of shear deficient R/C members. It is composed of three sub-elements accounting for flexural, shear and anchorage-slip deformations (Figure 1). The sub-elements are connected in series, hence the element flexibility matrix (F) is produced by the summation of the flexibility matrices of the flexural (F^{fl}), shear (F^{sh}) and anchorage-slip (F^{sl}) sub-elements and its inversion results in the element stiffness matrix K, which in turn relates the bending moment increments at the ends of the flexible part of the element to its incremental rotations (Figure 1):

$$K = F^{-1} = (F^{fl} + F^{sh} + F^{sl})^{-1} \tag{1}$$

$$\begin{bmatrix} \Delta M_A \\ \Delta M_B \end{bmatrix} = K \times \begin{bmatrix} \Delta \theta_A \\ \Delta \theta_B \end{bmatrix} \tag{2}$$

The flexural sub-element (Figure 1c) is divided into an elastic intermediate region and two end regions, where flexural yielding takes place. A spread inelasticity model is employed to follow the gradual inward penetration of flexural yielding from the ends of each sub-element. This model distinguishes between loading and unloading or reloading states of the end sections, leading respectively to different stiffness distributions in the end-regions [33].

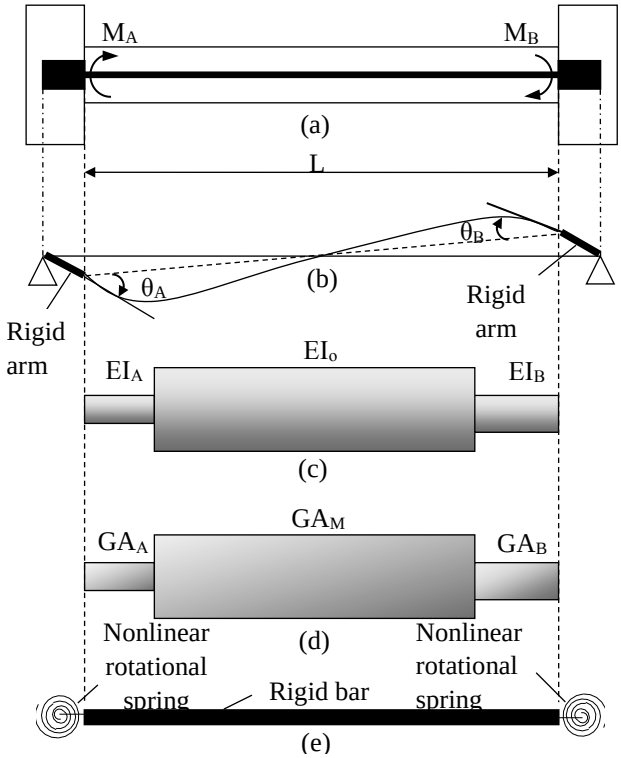

Figure 1: Finite element model: (a) geometry of R/C member; (b) beam–column finite element with rigid offsets; (c) flexural sub-element; (d) shear sub-element; (e) anchorage slip sub-element. [14]

The flexural sub-element's primary curve in terms of bending moment against curvature (M-φ) is based on standard flexural analysis with appropriate bilinearisation of the resulting curve. The rules followed for unloading are based on the model proposed by Sivaselvan & Reinhorn [34] with proper

modifications (described in detail in [14]), as shown in Figure 2a. Stiffness degradation during unloading and reloading as well as non-symmetric response (for cases of R/C T-beams) are accounted for in this flexural hysteretic model.

The anchorage slip sub-element represents the rotations arising at the interfaces of adjacent R/C members, due to slippage of the reinforcement anchorage in the joints, resulting from bond deterioration. The anchorage slip sub-element (Figure 1e) consists of two concentrated springs at the ends of the element, connected by a rigid bar, hence adding flexibility in the respective end, with its off-diagonal terms being zero [14]. Its bilinear primary curve in terms of bending moment vs. end rotations (M-θ_{slip}) is presented in detail in [14]; the hysteretic rules are based on the model proposed by Saatcioglu *et al.* [35], as shown in Figure 2b.

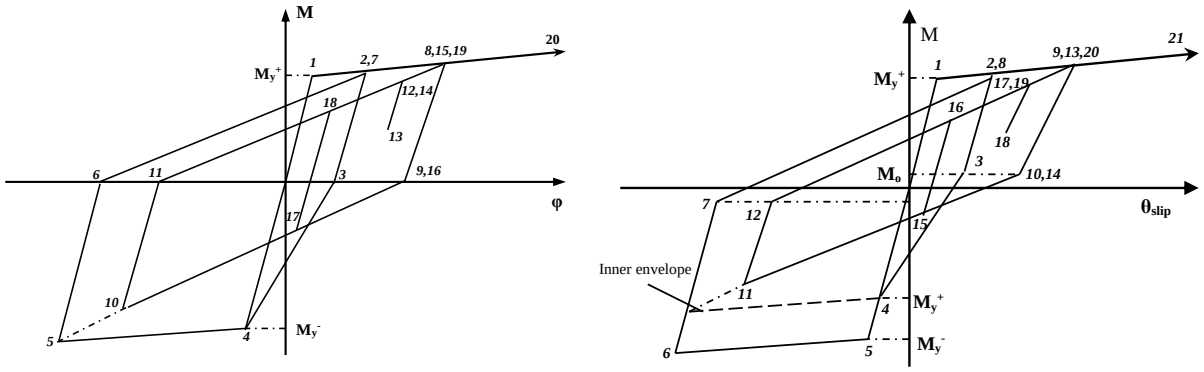

Figure 2: (a) Flexural (M-ϕ) hysteretic model and (b) anchorage slip (M-θ_{slip}) hysteretic model. [36]

Prior to the onset of shear failure, the shear sub-element has a flexibility distribution similar to the flexural sub-element (Figure 1d). Shear-flexure interaction is considered in its inelastic end regions, the lengths of which are set equal to the lengths of the respective regions of the flexural sub-element. The shear flexibility matrix coefficients are as follows (applying the principle of virtual work, see [14]):

$$f_{ij}^{sh} = \frac{a_{As}}{GA_A \times L} + \frac{1 - a_{As} - a_{Bs}}{GA_M \times L} + \frac{a_{Bs}}{GA_B \times L} \tag{3}$$

where $i,j = A, B$, i.e. the two ends of the element; α_{As} and α_{Bs} are defined as the yield penetration coefficients (Figure 3), which monitor the penetration of flexural yielding from the end A or B, respectively, towards the middle of the element; GA_A, GA_B and GA_M are the corresponding shear rigidities of end A, end B and the middle segment sections of the element; L is the element clear length.

Upon initiation of shear failure, localisation of shear strains is captured by setting the length of the region, where shear failure is detected, equal to the shear critical length L_{cr}. In line with experimental evidence, the shear failure plane is practically always unique, therefore the model invariably results in only one segment failing. For members where flexural yielding has developed prior to the onset of shear failure, the latter is expected to develop at the member ends due to the degradation of shear strength with inelastic flexural deformations. For members failing in shear without yielding in flexure, it is assumed that shear failure occurs in the middle region of the element. In Figure 3, the transition from pre-peak to post-peak regime for the generic cases of a flexure-shear and a shear critical specimen can be seen. The post-peak shear flexibility matrix coefficients with failure at the end A, at the middle of the element and at the end B, respectively, are as follows:

$$f_{ij}^{sh} = \frac{L_{cr}}{GA_A \times L^2} + \frac{1 - L_{cr}/L - a_{Bs}}{GA_M \times L} + \frac{a_{Bs}}{GA_B \times L} \tag{4}$$

$$f_{ij}^{sh} = \frac{1 - L_{cr}/L}{2 \times GA_A \times L} + \frac{L_{cr}}{GA_M \times L^2} + \frac{1 - L_{cr}/L}{2 \times GA_B \times L} \quad (5)$$

$$f_{ij}^{sh} = \frac{a_{As}}{GA_A \times L} + \frac{1 - a_{As} - L_{cr}/L}{GA_M \times L} + \frac{L_{cr}}{GA_B \times L^2} \quad (6)$$

Outside the critical shear length, only the pre-peak part of the shear hysteretic model described in [1] is applied. The pre-peak backbone curve modified for shear-flexure interaction effects is used in the regions that have yielded in flexure and the initial backbone curve for the rest of the element. Inside the critical shear length, the local, post-peak shear hysteretic model developed in [1] is applied. It is noted that this hysteretic model has been calibrated in terms of average post-peak shear strains within L_{cr}. Therefore, following this approach, the distribution and extent of shear deformations along the member length, before and after the onset of shear failure, is predicted in an accurate and objective manner. Furthermore, by considering the interaction of inelastic flexural and shear deformations at a local level, the proposed approach does not rely on assumptions regarding the bending moment distribution, hence the actual phenomenon is more realistically captured.

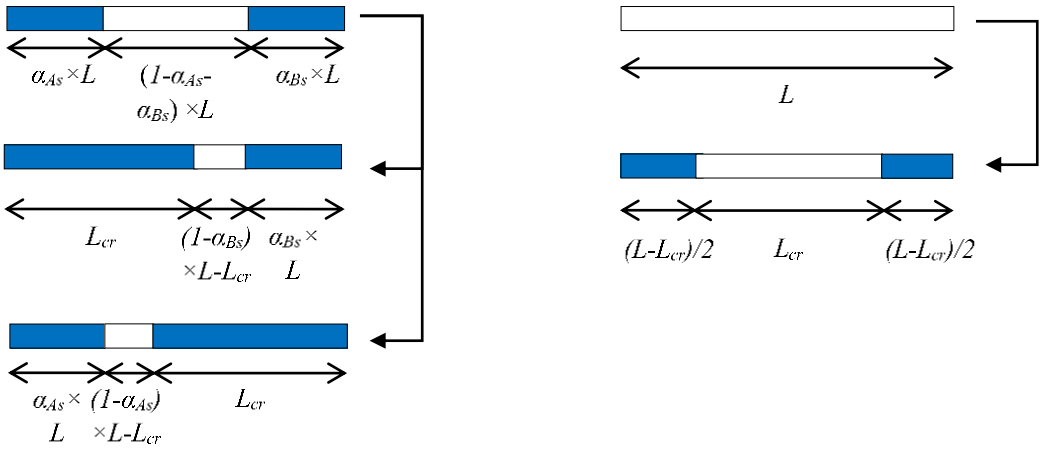

(a) (b)

Figure 3: Spread inelasticity transition upon initiation of shear failure for: (a) a flexure-shear critical specimen, and (b) a shear critical specimen.

3. FINITE ELEMENT MODEL IMPLEMENTATION

The beam-column model has been implemented in the general finite element program for inelastic dynamic analysis of structures IDARC2D [13], [37]. The prescribed post-peak V-γ descending branches [1] are followed subsequent to the onset of shear failure in the failed segment of the shear sub-element. This is realised by a commensurate drop in the current force, the yield strength, as well as the entire post-yield branch of the shear backbone, as shown schematically in Figure 4 with a linear descending branch, for the sake of clarity. This way, the stiffness is always positive, hence no instability occurs in the algorithm (note that IDARC cannot handle negative values of stiffness). The amount of strength degradation (ΔV_i with i=1,2…) at each solution step equals the 'over-shooting' of strength at the same step with respect to the strength of the target post-peak backbone branch with the same shear strain (see Figure 4). The strength degradation of each step is then applied in the next loading step as part of the "unbalanced forces". Using two independent branches in the bilinear descent (as in the shear hysteretic model [1]), the resulting response can be linear, concave or convex, encompassing all the different potential descending branch shapes, hence making the model more versatile and powerful.

Cyclic strength degradation in the post-peak domain should not create a shift of the resulting response towards the origin, i.e. a permanent loss of strength, which would distort the produced descending branch and lead to a slightly premature onset of axial failure in the case of shear strength reaching zero (Figure 5a). A compensation algorithm has been introduced to avoid this shift; instead of the second reloading branch aiming at the previous maximum point with a reduced strength, it extends to the intersection of the second reloading branch and the target backbone descending branch, similarly to what was originally proposed for the pre-peak response [38]; hence, the resulting behaviour is as intended (Figure 5b), in line with calibration of the post-peak degrading response [1].

The rest of the sub-elements (flexural, anchorage-slip) as well as the two non-failed segments of the shear sub-element (Figure 1) unload in parallel with the failed shear section's softening response, during in-cycle strength degradation. Were they to unload normally, they would alter the target lateral displacement $\delta_{lateral}$ response by producing opposite displacements. This is not consistent with the assumption made when calibrating the local shear hysteretic model [1], where it is assumed that all other displacements apart from the shear displacements in L_{cr} remain practically constant after the onset of shear failure. Therefore, this will lead to an ostensibly steeper slope in the shear force - lateral displacement relationship as shown in Figure 6 with S'_{pp} representing the slope of the target descending backbone branch and S'_{error} a steeper, erroneous slope, both in terms of V- $\delta_{lateral}$.

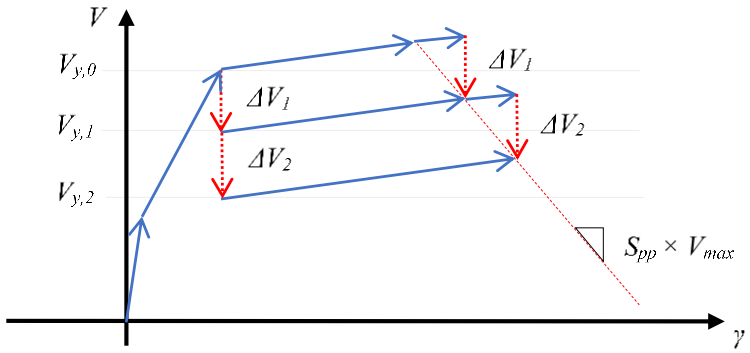

Figure 4: Schematic representation of the implementation of in-cycle degradation.

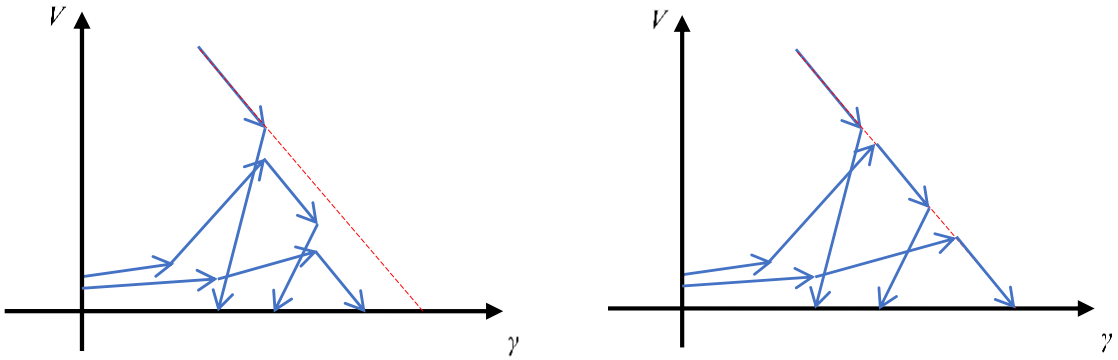

(a) (b)

Figure 5: Schematic representation of (a) the shear response with descending branch offset due to cyclic degradation and (b) the response with compensation for this offset.

In previous models ([9], [39]), the slope of the shear sub-element's descending branch was modified based on the unloading stiffness of the other sub-elements, in order to tackle this problem. Herein, however, for the formulation to be consistent with the theoretical basis of this model, i.e. all the post-peak lateral displacements being ascribed to the shear response, a very high unloading stiffness is assigned to the other sub-elements and the other segments of the shear sub-element, while the failed shear section is in contact with the descending branch (Figure 6). This ensures that the intended lateral

displacement response is achieved.

Another issue of similar nature is the shift of the response which occurs in reloading, due to the other sub-elements connected in series aiming at their previous vertex points, while the failed section aims at a degraded strength (Figure 7). This has been reported elsewhere in the past and was dealt with using a compensation algorithm that adjusts the shear reloading stiffness and backbone, so that the desired response is produced [39]. A simpler and more intuitive solution was preferred herein. The strength degrades uniformly in the whole system; in other words, the strength degradation of the failed shear section (both in-cycle and cyclic) is also inflicted on the rest of the sub-elements and sections of the shear sub-element. Thus, they target their degraded vertex point in reloading, hence not producing this shift in response in the first place (Figure 7).

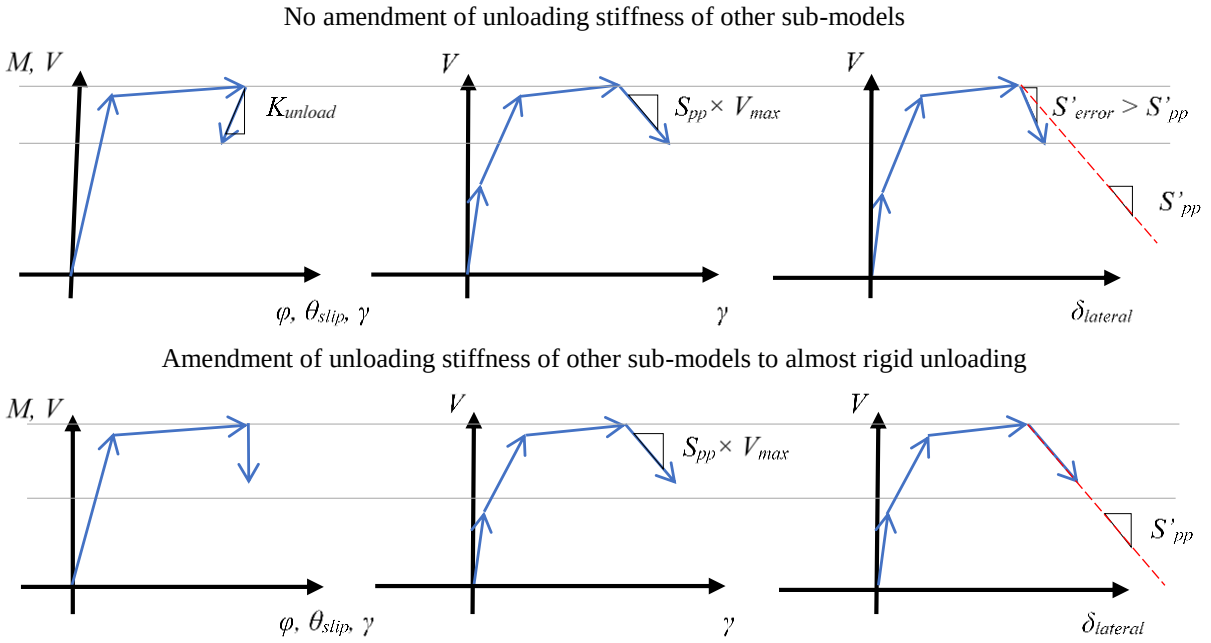

Figure 6: Schematic representation of the influence of unloading stiffness of the other sub-models (left) simultaneously with in-cycle strength degradation of failed section (middle) on the shear force vs lateral displacement response (right).

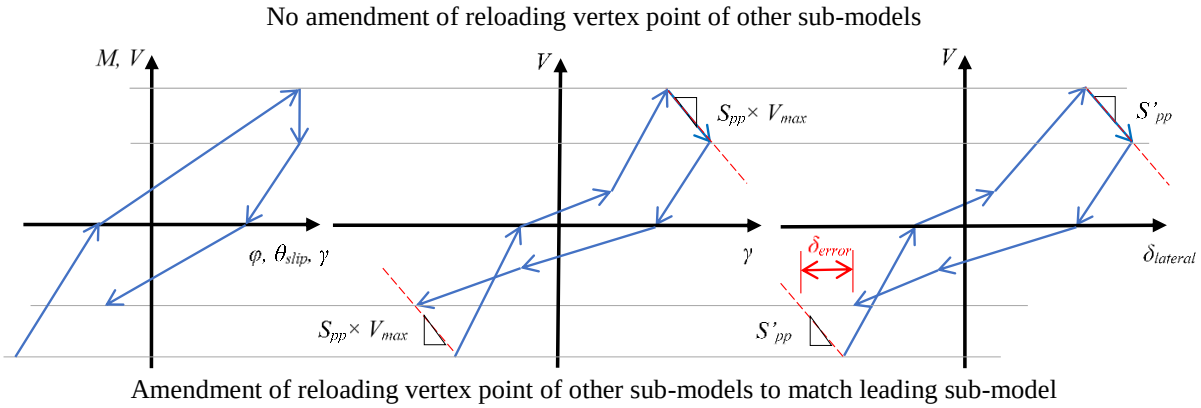

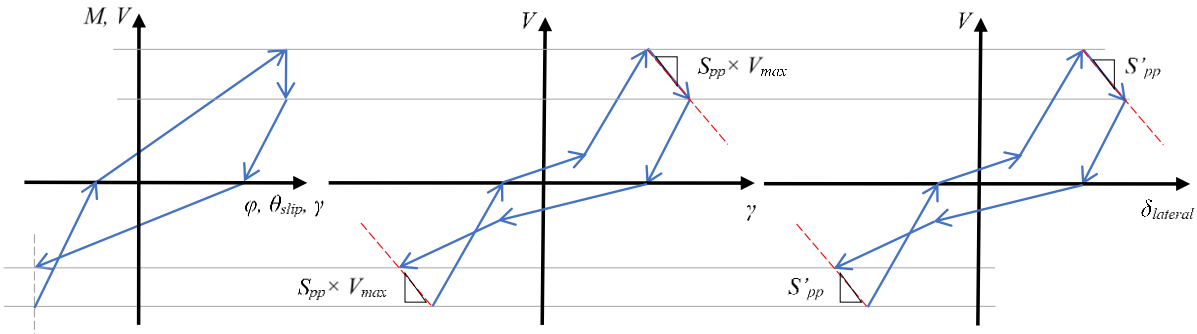

Figure 7: Schematic representation of influence of reloading of the other sub-models (left) simultaneously with reloading of the failed section (middle) on the shear force - lateral displacement response (right).

The beam-column axial failure subsequent to shear failure is both deformation-based and force-based in the proposed formulation. Specifically, the element is considered to have failed axially after shear failure, if either the shear deformation limit corresponding to the onset of axial failure has been reached ($\gamma_{sh,f} + \gamma_{t,pp}$ in [1]) or the element's shear strength has degraded to zero. Flexural and anchorage failures are determined by exceedance of the ultimate curvature and bond-slip end rotations, respectively.

4. FINITE ELEMENT MODEL VERIFICATION

Verifications of the finite element model with various experimental results are provided in this section. More verifications can be found in [40].

4.1 Accuracy of analytical prediction

The accuracy of analytical predictions is often presented and judged on a visual basis, i.e. through comparison of resulting diagrams. While this is reasonable, it provides by no means an objective metric so as to compare the performance among different models.

Herein, inspired by a recent study [41], objective accuracy measures are proposed, so that the results can be comparable with future analytical predictions. All the ratios have the numerical value as numerator and the experimental one as denominator. The following are deemed important for the current application, hence are computed and presented:

- Energy Dissipation Ratio (R_E).
- Shear Failure Displacement Ratio (R_{SFD}), i.e. the displacement at the onset of shear failure.
- Axial Failure Displacement Ratio (R_{AFD}), wherever applicable, i.e. wherever axial failure initiation was recorded.

4.2 Flexure-Shear Critical Specimens

Sezen & Moehle [42] tested four double-curvature columns with different axial loads under quasi-static cyclic loading. They were lightly reinforced, representative of old-type construction, designed to yield in flexure and subsequently fail in shear. The column Specimen-1, tested under an axial load of 667 kN (v = 0.15), is selected for verification of the proposed analytical model. Its clear height was 2946 mm, with a 457 mm square cross-section and a longitudinal reinforcement ratio of 2.5%. The transverse reinforcement comprised rectangular and diamond-shaped ties at 305 mm spacing, with 90° anchorage hooks (Figure 8). The concrete compressive strength was 21 MPa and the longitudinal and transverse reinforcement yield strengths were 434 MPa and 476 MPa, respectively.

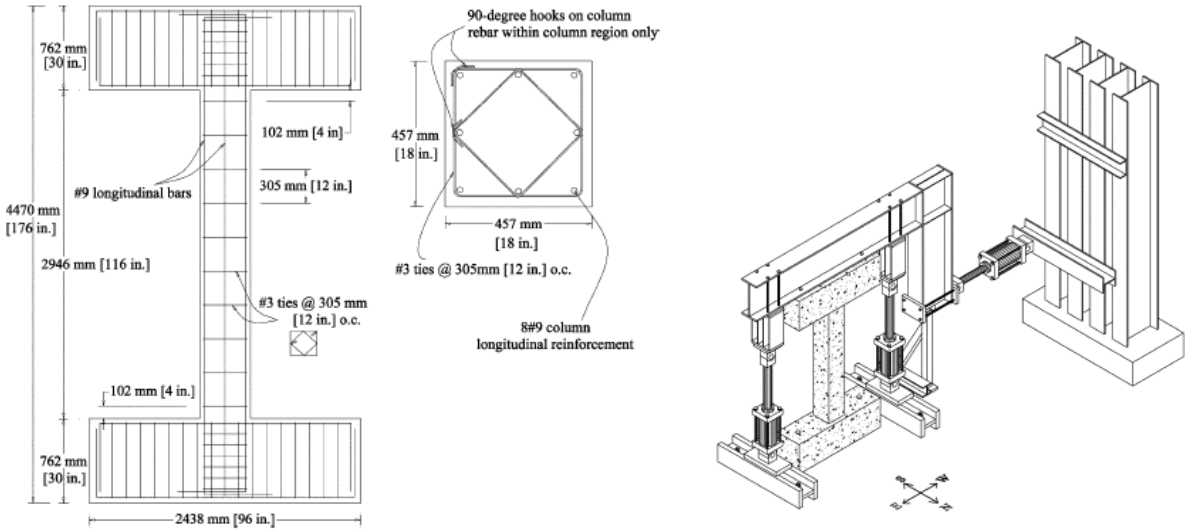

(a) (b)

Figure 8: (a) Specimen-1 details and (b) test set-up. [42]

The proposed model seems to be capturing the pre- and post-peak hysteretic response fairly well (Figure 9a). It matches very well the overall behaviour, with unloading and reloading stiffnesses of the analysis representing well the average stiffnesses observed experimentally, capturing very well the high strength degradation at the displacement level of ±82 mm. Of course, there is some discrepancy at given points.

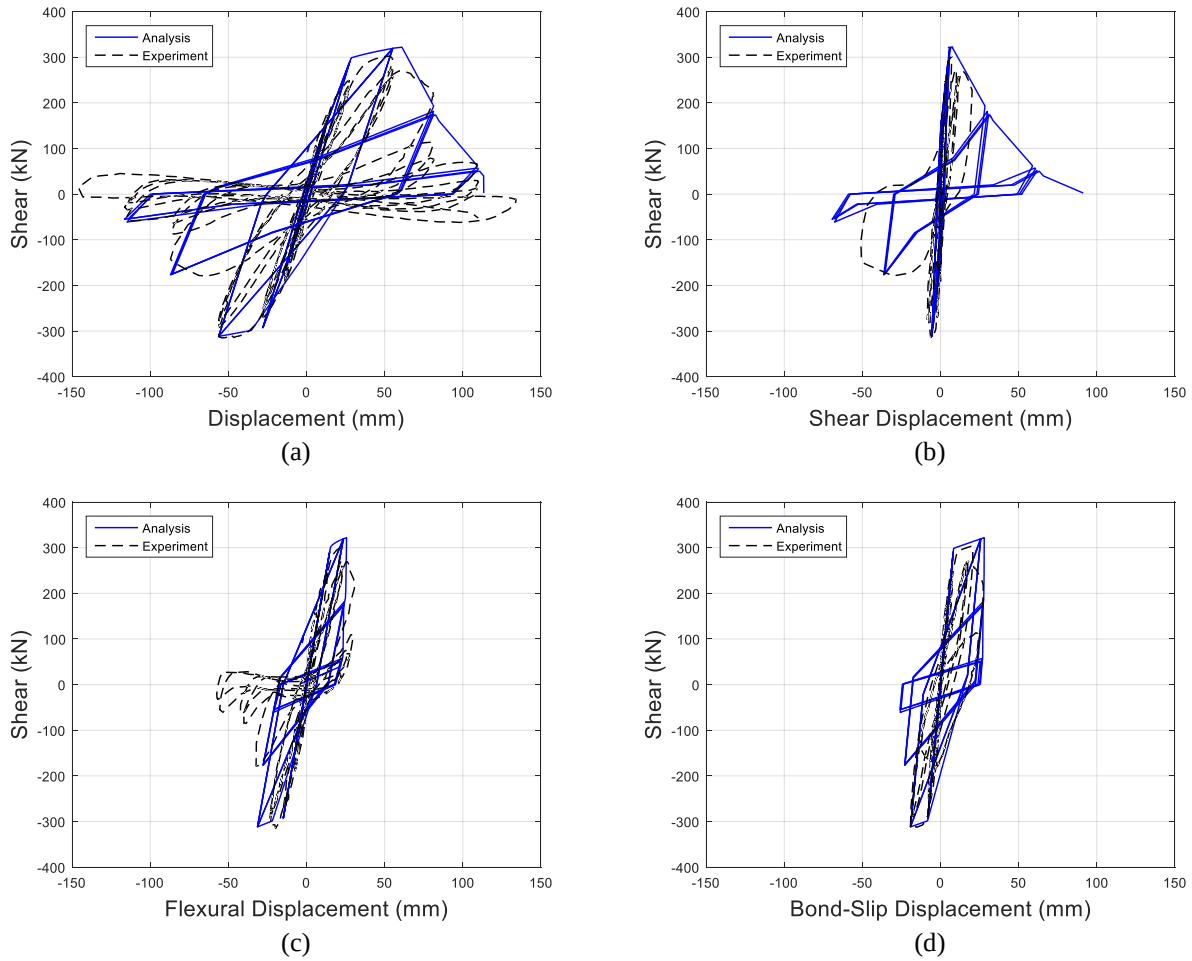

(a) (b)

(c) (d)

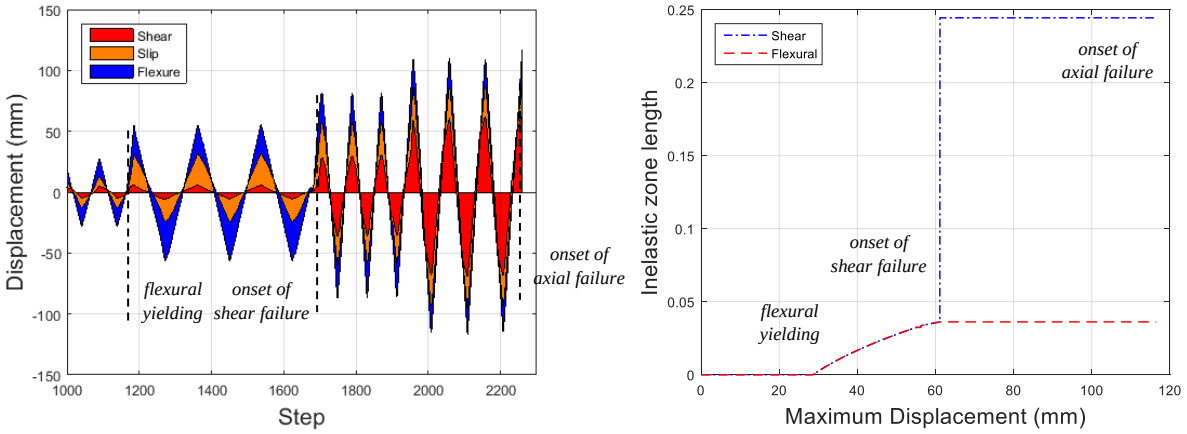

(e) (f)

Figure 9: Comparison between the predicted response by the proposed model and the experimental one in terms of (a) shear force against lateral displacement, (b) shear displacement, (c) flexural displacement and (d) anchorage slip displacement. (e) Lateral displacement decomposition, and (f) flexural and shear inelastic zone lengths normalised by the clear member length, during the analysis.

Contrasting the predicted values with the experimental ones (Table 1), the displacement at the onset of shear failure is predicted quite well, with some overestimation. The onset of axial failure is predicted at the last displacement level; the R_{AFD} (Table 1) shows about 20% underestimation of the expected deformation, however. This is due to the fact that the descending branch was found to be slightly steeper than its experimental counterpart; at the same time, strength in the last cycles seems to be reaching negative values in the experimental response, which is a failure criterion for the analytical model as previously explained. Energy dissipation is shown to be overestimated compared to the actual energy dissipated by the member during the cyclic test.

Lateral displacement components are captured very well both in the pre- and post-peak domains (Figure 9b-d), given the challenge of predicting individual displacement components in lieu of total displacements in displacement-controlled experiments. There is a negligible underestimation of shear deformations before the peak; upon shear failure the shear displacement increases considerably in the positive direction, a tendency which the model captures adequately. There is slight underestimation of shear displacements on the subsequent negative side. Not all shear response history is provided by the researchers [42], possibly due to failure of the recording instrument. Therefore, only one full experimental post-peak cycle is presented in Figure 9b, whilst the entire analytical response is provided. Anchorage slip displacement (Figure 9c) is predicted with very high accuracy, with the sole exception of the first negative post-peak half-cycle, where there is slight overestimation. The predicted response shows good agreement with the experiment in the pre-peak flexural response (Figure 9d), with reasonable deviation in the post-peak; the experimental post-peak flexural displacement seems to be biased towards the negative side, increasing substantially in the latter post-peak cycles. As has been reported in [11], a hysteretic macro-model's objective should be to capture each individual component as accurately as possible, rather than merely predicting the total response. However, this has rarely been reported in previous studies, possibly due to scarcity of experimental programmes reporting separate deformation components, the reliability of measured recordings that can be highly dependent on setup, methodology and instrumentation, or due to inability of some models to predict them accurately, relying on aggregation of overestimated and underestimated components to provide a fair total response. Achieving such level of agreement with separate experimental displacement components can be considered a very positive indication for an analytical model.

Figure 9e shows the analysis of the components of the lateral displacement of the element (only part of the response is shown, for the sake of clarity). Shear displacements are naturally very low at the first stages of the response, increasing significantly after the element yields, due to shear-flexure interaction

at the ends of the member. Furthermore, they increase drastically after the onset of shear failure, as all post-peak displacements are attributed to the shear sub-element; the flexural and bond-slip displacements, on the other hand, do not exceed their maximum pre-peak values at any point in the post-peak domain. Figure 9f demonstrates the spread of inelasticity during the analysis for the flexural and shear sub-elements. After flexural yielding, the inelastic zones increase following the bending moment increase at the member ends, always being equal. As soon as the onset of shear failure is reached just after the maximum displacement of 60 mm, the inelastic zone of the shear sub-element instantly assumes a value corresponding to the shear critical length, where the diagonal shear failure plane forms, and maintains it for the remaining of the analysis. Simultaneously, the inelastic zone of the flexural sub-element remains equal to the maximum value it has reached up to the onset of shear failure.

Table 1: Accuracy measures of the analysis of Specimen-1, C-2, SC3 and Frame 1.

	R_E	R_{SFD}	R_{AFD}
Specimen-1	**1.362**	**1.086**	**0.797**
C-2	**0.858**	**0.571**	**N/A**
SC3	**1.241**	**1.103**	**N/A**
Frame 1	**0.852**	**1.152**	**N/A**

Lejano *et al*. [43] conducted an experimental programme to study the deformation characteristics of short double-curvature R/C columns with high-strength concrete under quasi-static cyclic loading as well as high or fluctuating axial load. The specimen C-2 is herein selected for analysis, having a 278 mm square cross-section and a length of 646 mm, with high longitudinal and transverse reinforcement ratios of almost 4% and 1%, respectively (Figure 10). The steels used have a yielding strength of 496.2 and 414.0 MPa, respectively, while the high-strength concrete 39.6 MPa. It is subjected to unusually high compressive axial load, i.e. an axial load ratio ($v = N / A_g \times f_c$) of approximately 0.80.

The proposed model captures the pre- and post-peak hysteretic response very accurately (Figure 11a). The overall behaviour is matched very well, with unloading and reloading stiffnesses of the analysis closely capturing the average stiffnesses observed experimentally. The onset of shear failure is predicted slightly earlier, mainly due to the ductility of the specimen after yielding, which is more limited in the analytical prediction; this can also be seen in Figure 11c, where the overall flexural and bond-slip analytical response exhibits very limited inelasticity, while the experimental one exhibits a relatively larger – yet still low – inelastic deformation component. Strength degradation follows very closely the apparent descending branch of the response, deviating slightly only in the last positive half-cycle; in addition, post-peak cyclic strength degradation is accurately captured.

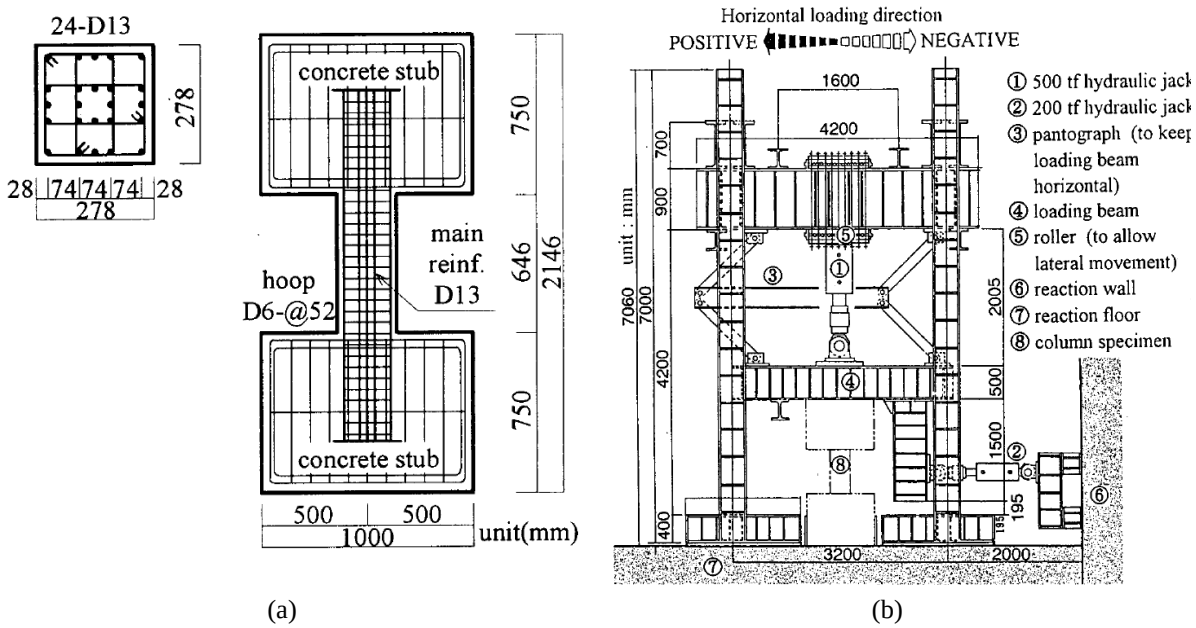

(a) (b)

Figure 10: (a) Specimen C-2 details and (b) test set-up. [43]

Comparing the predicted values with the experimental ones (Table 1), the displacement at the onset of shear failure seems to be underestimated considerably based on R_{SFD}. However, in absolute terms the difference is not so significant, hence not influencing adversely the descending branch and the subsequent response. The maximum displacement reached is predicted to be lower than the actual one, i.e. about 13 mm, while the experimental test reaches 20 mm without axial failure. This is, of course, attributed to the extremely high axial load ratio value, which leads to a prediction of very low deformability. Probably the high longitudinal and transverse reinforcement contributed to reaching such displacement capacity during the experiment, which was not reflected appropriately by the empirical relationship.

Energy dissipation is negligibly underestimated compared to the actual energy dissipated by the member during the cycling (Table 1). Nevertheless, Figure 11d shows that the analytically predicted energy dissipation is very close to the experimental one at all stages of the analysis, generally being underestimated more in the pre-peak domain, due to the aforementioned underestimation of ductility in the first cycles and some dissipation of the experiment during the initial cycles which is considered completely elastic behaviour by the analytical model. Once the post-peak domain is entered, the energy is slightly overestimated, mainly due to underprediction of pinching, making up for the pre-peak deficit and reaching practically the same total dissipated energy by the displacement of 13 mm. The experimental energy keeps rising after that, leading to the aforementioned discrepancy owing to the higher displacement capacity of the member.

Figure 11b-c show separately the shear as well as flexural and bond-slip responses. It can be seen that both of them are very well predicted. The marked increase of shear displacement with simultaneous limiting of the other components is very clear, confirming once again the fact that shear displacement increases drastically after the onset of shear failure, while the other components are essentially capped. Flexural and bond-slip response seems to have a ratcheting asymmetric behaviour beyond shear failure skewed towards the positive side, which is not captured by the analytical model; in turn, this leads to an asymmetry in the shear response towards the negative side, resulting in the model overestimating the positive side shear deformations while underestimating the negative.

The inelastic lengths' behaviour is similar to the one of the previous specimen, hence not included. The flexural inelastic zone, however, is very limited (less than 1% of the column length), owing to the very limited curvature ductility of the specimen.

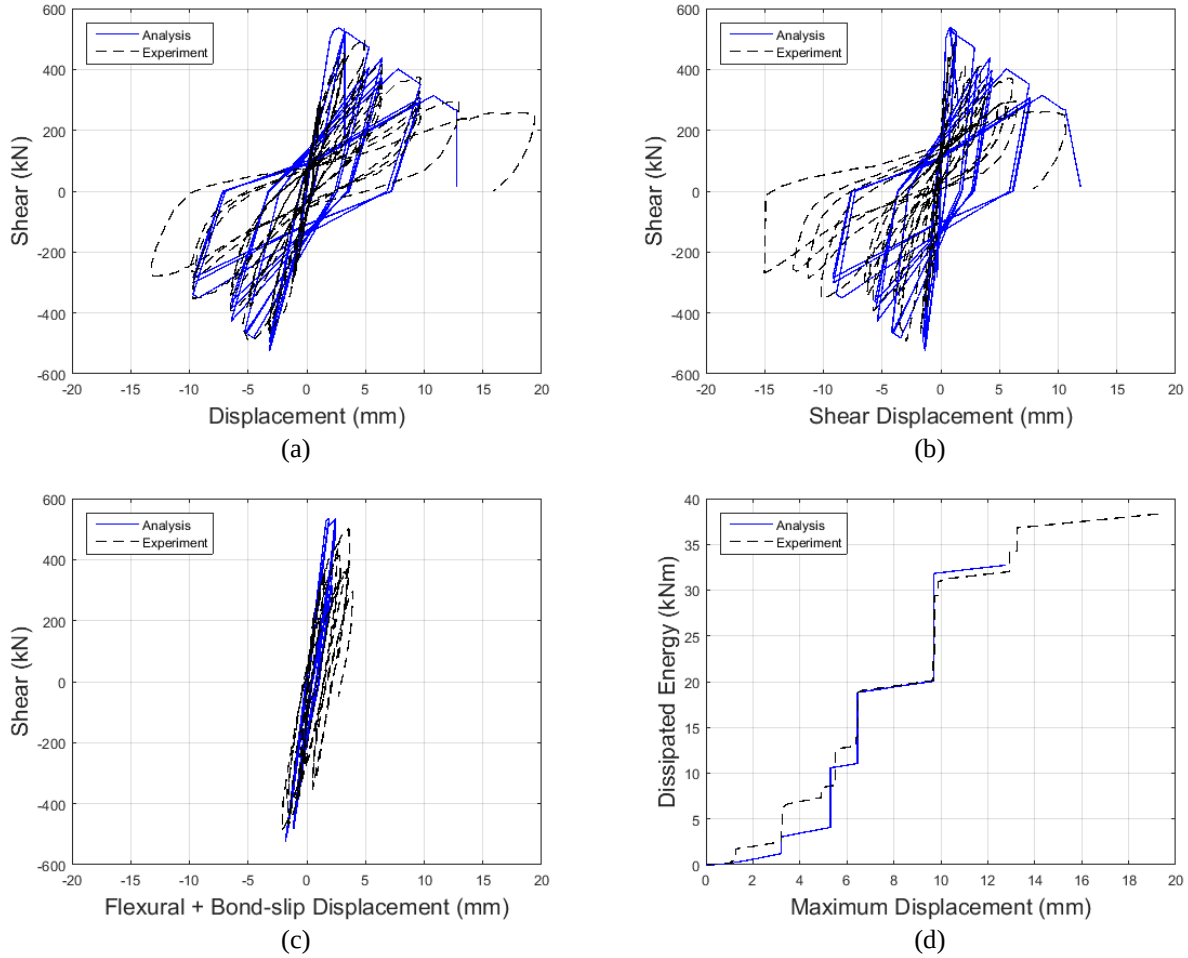

Figure 11: Comparison between the predicted response by the proposed model and the experimental one in terms of (a) shear force against lateral displacement, (b) shear displacement and (c) flexural and bond-slip displacement; (d) cumulative dissipated energy during the analysis.

It is noteworthy that disregarding the post-peak response of this specimen, e.g. using an analytical model considering 15% or 20% strength degradation as failure, the deformability of the specimen would be gravely underestimated, predicting a maximum displacement of about 5 mm, whilst the column is shown to be able to reach 20 mm, a fourfold displacement, barely losing half its lateral strength. This highlights once more the importance of modelling the full-range response of substandard R/C elements in cases where the collapse limit state has to be considered.

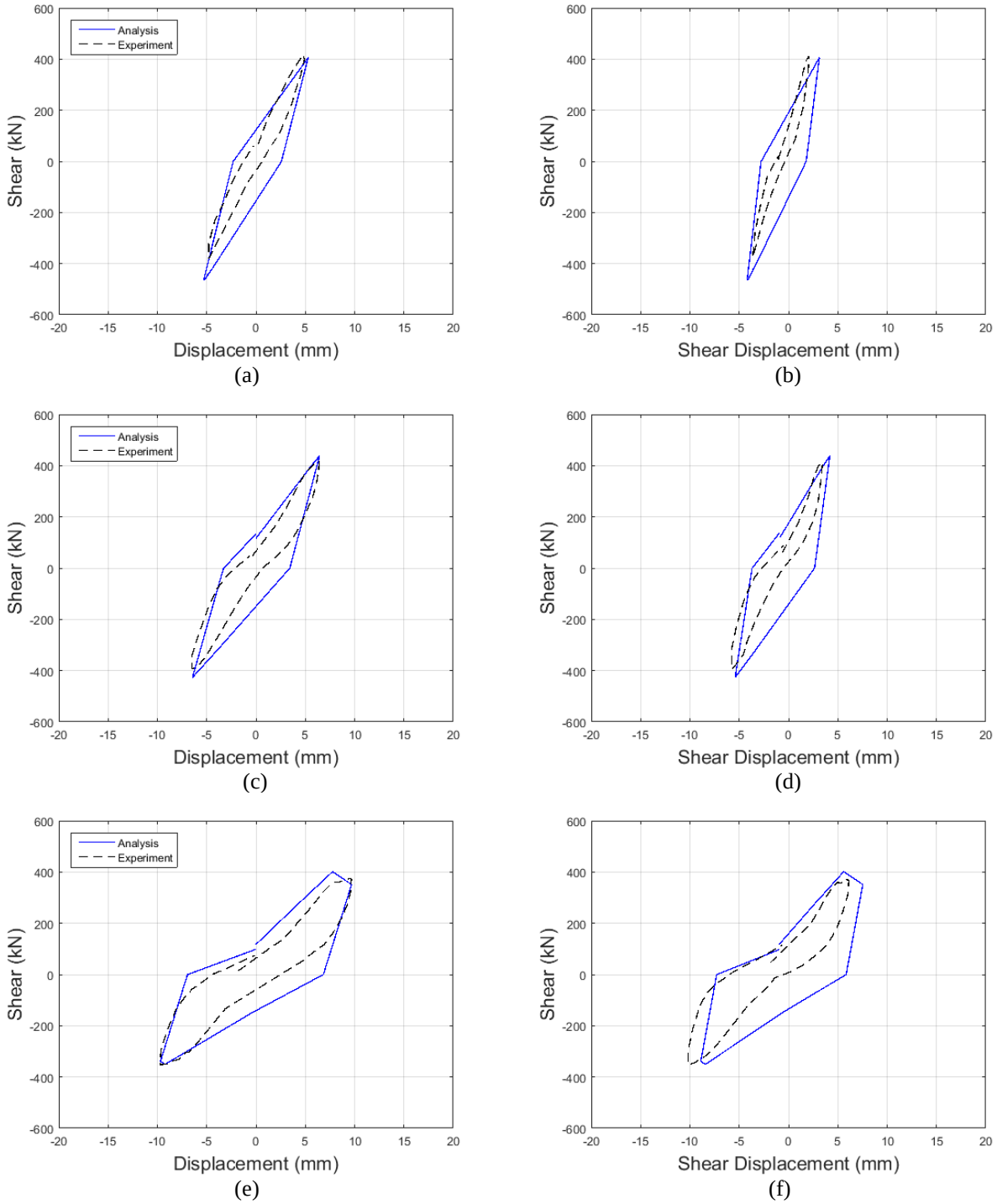

Figure 12: Comparison between individual cycles of the predicted response of C-2 by the proposed model and the experimental one: (a, b) 2nd cycle at +/- 5 mm, (c, d) 1st cycle at +/- 6.5 mm, and (e, f) 1st cycle at +/- 10 mm. (left) Total displacements and (right) shear displacements.

Figure 12 shows comparisons of selected individual hysteretic cycles of the analytical response against the experimental one, in the post-peak domain of the response. The total displacement analytical cycles are found to agree very well with the experimental ones. The unloading and reloading stiffness in each cycle match the experimentally recorded ones on average. The strength degradation inflicted upon the specimen with increasing displacement and cycles seems to be followed very well. Pinching is observed in the advanced displacement levels of the experimental response (e.g. Figure 12c, e), which however is underestimated in the analytical prediction and is only slightly captured in the very last

analytical cycles not shown here. The energy dissipated along each analytical cycle can be seen to be greater than the corresponding experimental ones, largely due to the aforementioned underprediction of pinching, leading to thicker loops. The shear displacement cycles of the analysis also show good agreement, once more being thicker than the experimental ones, though.

4.3 Shear Critical Specimen

Aboutaha *et al.* [44] tested 11 large-scale short columns, investigating the effect of various rectangular steel jacket types on strength and ductility of columns with inadequate shear strength. Three of them were tested before retrofit as reference response. Herein the unretrofitted cantilever specimen SC3 is examined, which failed in shear before yielding in flexure. Its clear height was 1219 mm, with a section 914×457 (mm) and a longitudinal reinforcement ratio of 1.9%. It was subjected to uniaxial cyclic loading in its weak direction. Its transverse reinforcement comprised rectangular perimeter ties combined with cross ties, spaced at 406 mm. The concrete compressive strength was 21.9 MPa and the yield strengths of longitudinal and transverse reinforcement were 434 MPa and 400 MPa, respectively.

The proposed model captures the pre- and post-peak hysteretic response well (Figure 13a). The plateau from ±10 mm to approximately ±23 mm is very well captured and unloading and reloading stiffnesses are on a par with the experimental ones. The onset of shear failure is predicted slightly later than the experimental one and the predicted post-peak descending branch underestimates the experimental strength degradation to some extent, especially on the positive side.

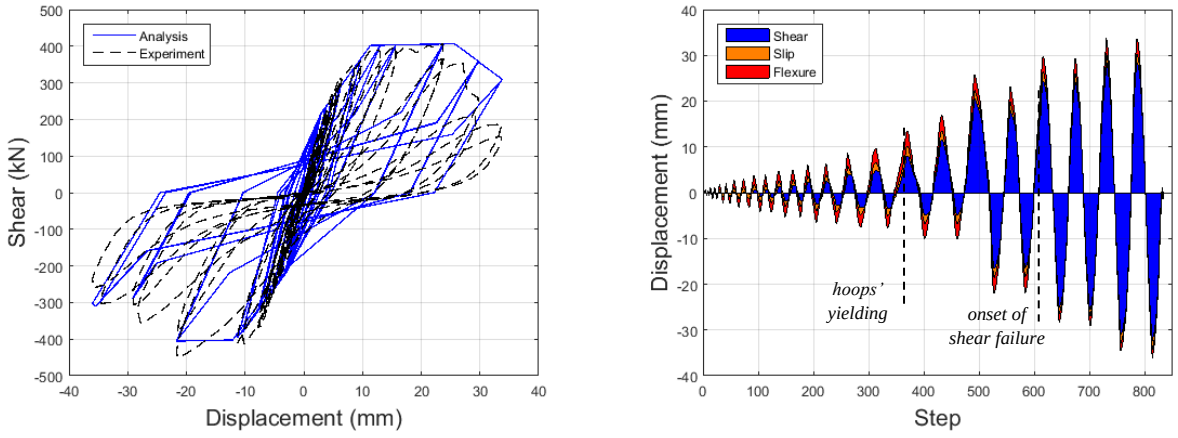

Figure 13: Aboutaha et al.'s [44] SC3 specimen: (a) Comparison between the predicted response by the proposed model and the experimental one in terms of shear force against lateral displacement. (b) Lateral displacement decomposition.

Comparing the predicted values with the experimental ones (Table 1), the displacement at the onset of shear failure is overestimated by about 10% (Figure 13a). The maximum displacement reached is precisely predicted, as the model did not underestimate the onset of axial failure neither overestimated the in-cycle strength degradation of the test, hence reaching the final step of the displacement history and correctly predicting that the specimen does not fail axially during the test. Energy dissipation is predicted with about 24% overestimation compared to the actual energy dissipated by the member during the test. This discrepancy is mainly attributed to the aforementioned delayed onset of shear failure and low predicted strength degradation, as well as the extreme pinching behaviour observed in the post-peak experimental response. Although the model also predicts substantial pinching, it does not capture its actual extend.

Figure 13b shows the decomposition of lateral displacement components. The member being shear critical, shear-induced displacements are naturally a significant part of the total displacement from the early stages of the response. Nonetheless, they increase drastically as a percentage of the total after the

onset of shear failure, as all post-peak displacements are localised at the shear sub-component; the flexural and bond-slip displacements, on the other hand, do not exceed their maximum pre-peak values at any point in the post-peak domain, thus decreasing significantly as a percentage of the total lateral displacement.

4.4 Frame specimen

Elwood & Moehle [45] carried out shake-table tests on two R/C frames to study shear followed by axial failure and the redistribution of vertical loads in neighbouring elements of an R/C sub-assembly. They were both three-column one-storey frames, with two well-designed circular columns at the edges and a rectangular shear-deficient column in the middle, supported on large footings at the bottom and connected at the top via a 1.5 m wide beam (Figure 14a). The specimen Frame 1 is examined herein, which was carrying a total mass of 31 t, resulting in a weight of 128 kN carried by the centre column. The latter had a 230 mm square section, being a ½-scale mock-up of the column analysed above (Specimen-1). It had a longitudinal reinforcement ratio of 2.5% and a transverse reinforcement ratio of 0.18% consisting of rectangular and diamond-shaped ties with 90º anchorage hooks. The concrete compressive strength was 24.5 MPa and the longitudinal and transverse reinforcement yield strengths were 479 MPa and 718 MPa, respectively. The outside columns were detailed with closely-spaced spiral hoops leading to very high confinement, ensuring that when the axial support of the mid-column is lost, these columns will be capable of supporting the redistributed gravity loads. The specimen was subjected to a horizontal component of a scaled ground motion of the 1985 Chile earthquake recorded at Viña del Mar (Figure 14b). Before the main shaking, it was subjected to an accelerogram scaled to 13% of this one, the frame remaining elastic throughout, thus this has not been modelled herein.

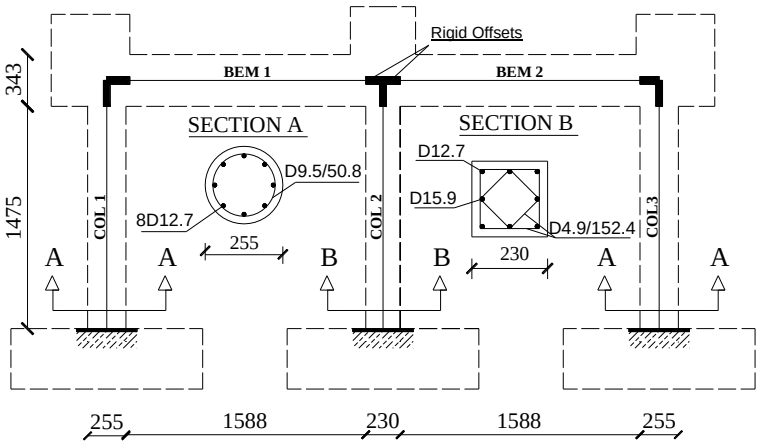

(a)

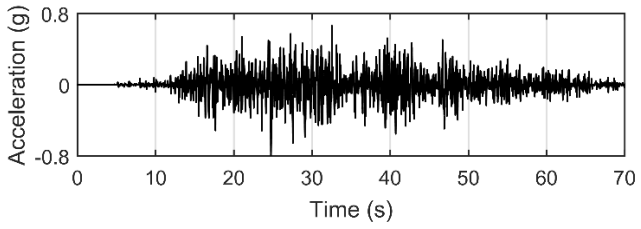

(b)

Figure 14: (a) Frame 1 layout (dimensions in mm) and applied finite element model [14]; (b) applied accelerogram.

This case puts the model's capabilities to the test, as it is both an R/C sub-assembly instead of an individual member and an actual dynamic analysis instead of a quasi-static one. The finite element model applied herein for the inelastic response-history analysis of the R/C frame is shown in Figure 14a. It consists of three column elements and two beam elements, keeping the minimal number of finite elements required, ensuring low computational cost [14]. The columns are assumed to be fixed at the

bottom. Rigid offsets are employed to model the joints of the frame. Viscous damping is modelled using the Rayleigh model with an equivalent viscous damping equal to 2% of critical for the fundamental vibration mode, as suggested by free-vibration tests conducted before the test [45]. The mass has been assumed lumped at the top of the frame.

The response histories of the lateral displacement of the first storey as well as the base shear of the frame are shown in Figure 15. The hysteretic response of the entire R/C frame and the middle column, the cumulative energy dissipation of the frame, as well as hysteretic local shear deformations of the mid-column, are presented in Figure 16. A triangular marker is inserted in every diagram of Figure 15 and Figure 16 to signal the onset of shear failure of the middle column. Part of the response is omitted in Figure 15 for the sake of clarity, i.e. before 10 s, as it has also been reported in detail in [14], and after 55 s, as it consists of very low amplitude cycles, fading out to the eventual resting position of the frame. In Figure 16a,b and d, the more critical part of the response is shown, i.e. between 15 s and 35 s, for the sake of clarity.

Shear failure took place at the top of the middle column during the analysis, in line with photographic evidence of the damage (Figure 17a), subsequent to flexural yielding of the column. The predicted shear-damaged zone and bottom plastic hinge are shown in an illustration of the damage, based on the analytical results, in Figure 17b; the entire length of the column was predicted to have shear cracking. The other two columns yielded slightly sooner than the middle column as in the experimental test. The key point of the onset of shear failure of the mid-column is predicted very accurately at 16.7 s.

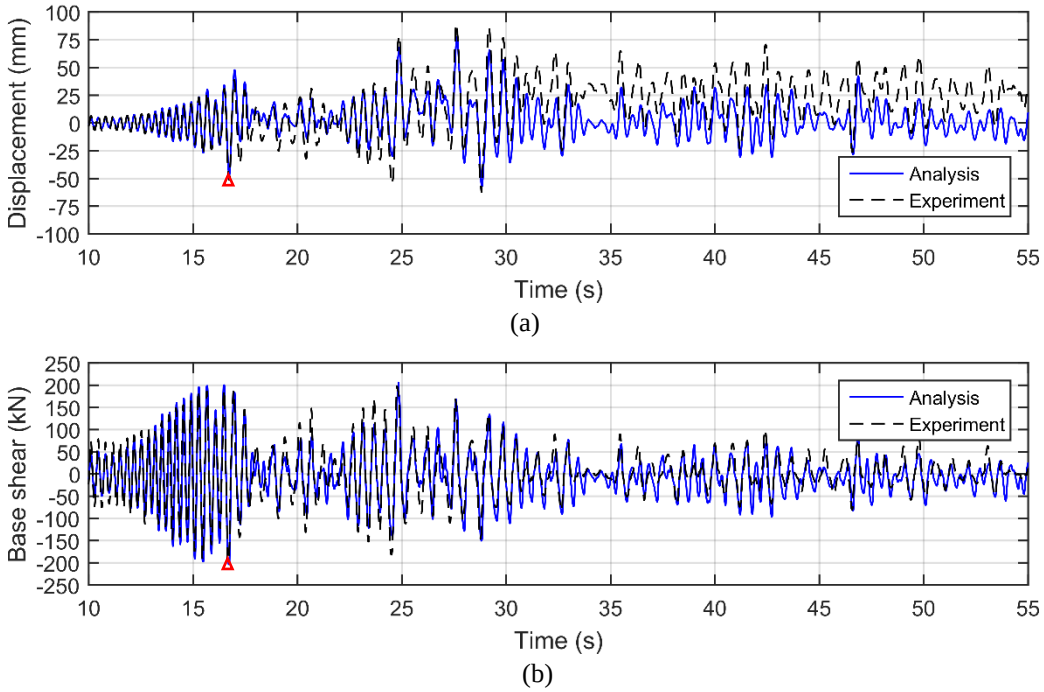

Figure 15: Comparison between response history predicted by the proposed model and the experimental test in terms of (a) lateral displacement of the frame's first storey as well as (b) its base shear.

As can be seen in Figure 15, the experimentally obtained and analytically predicted lateral displacements are on a par up to about 30 s, achieving very good agreement. Thenceafter, there is a shift of the experimental displacements to +30 mm that remains even after the end of the test as a residual lateral displacement, which the analysis does not capture; this discrepancy is in accord with analytical results published by the same research team that conducted the experiments [46]. This highlights the open challenges in correctly predicting the residual displacements of such R/C sub-assemblages and the complexity of non-linear dynamic analyses. Except for this discrepancy, the analytical response resembles very closely the experimental one. The shear failure (Table 1) and maximum lateral displacement predictions are fairly good with over- and under-estimation of about 15%, respectively.

With regard to base shear, the predicted response seems to be even more accurate, closely observing the experimentally obtained one before and after the initiation of shear failure.

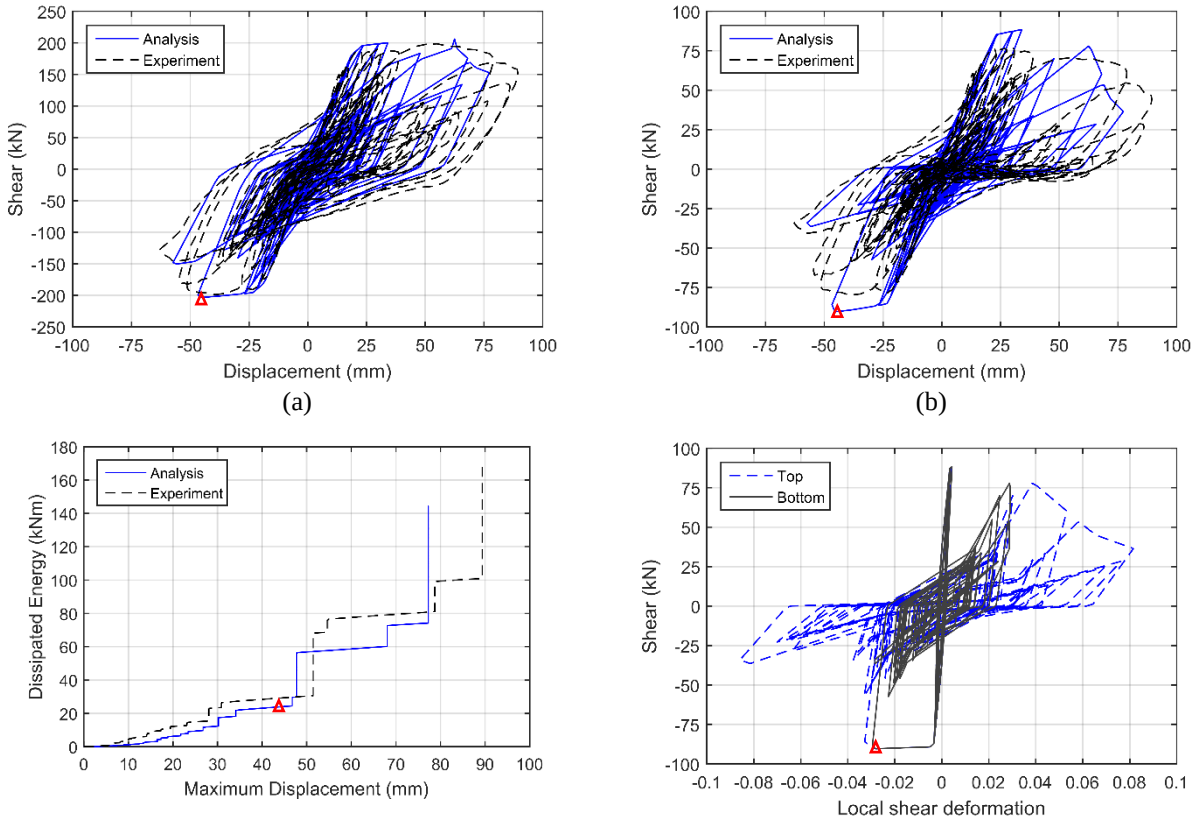

Figure 16: Comparison between predicted response by the proposed model and the experimental test in terms of (a) base shear against lateral displacement of the first storey of the frame and (b) shear force against lateral displacement of the middle column; (c) cumulative dissipated energy during the analysis; (d) shear force against local shear deformation (γ) of the top and bottom segments of the mid-column.

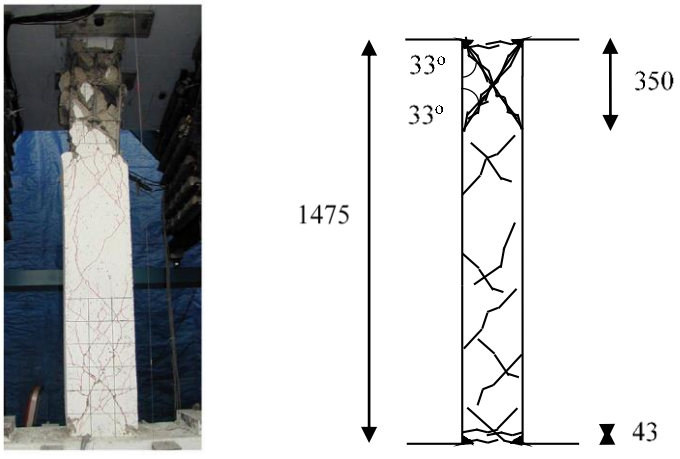

Figure 17: (a) Photographic documentation of the damage sustained by Frame 1 [45]; (b) predicted damage by the proposed model.

The analytical and experimental hysteretic responses (Figure 16a) show very close agreement, the onset of shear failure and the ensuing shear strength degradation are predicted very well and the resulting analytical cyclic envelope coincides fairly well with the experimental one. This good match can also be seen in Figure 16b in the hysteretic response of the middle column. Its maximum strength is slightly

overestimated; however, a fairly good prediction of the expected overall behaviour is attained. Despite the fact that the displacements of some large-amplitude cycles are somewhat underestimated, the post-peak strength degradation follows very well the experimentally measured shear resistance.

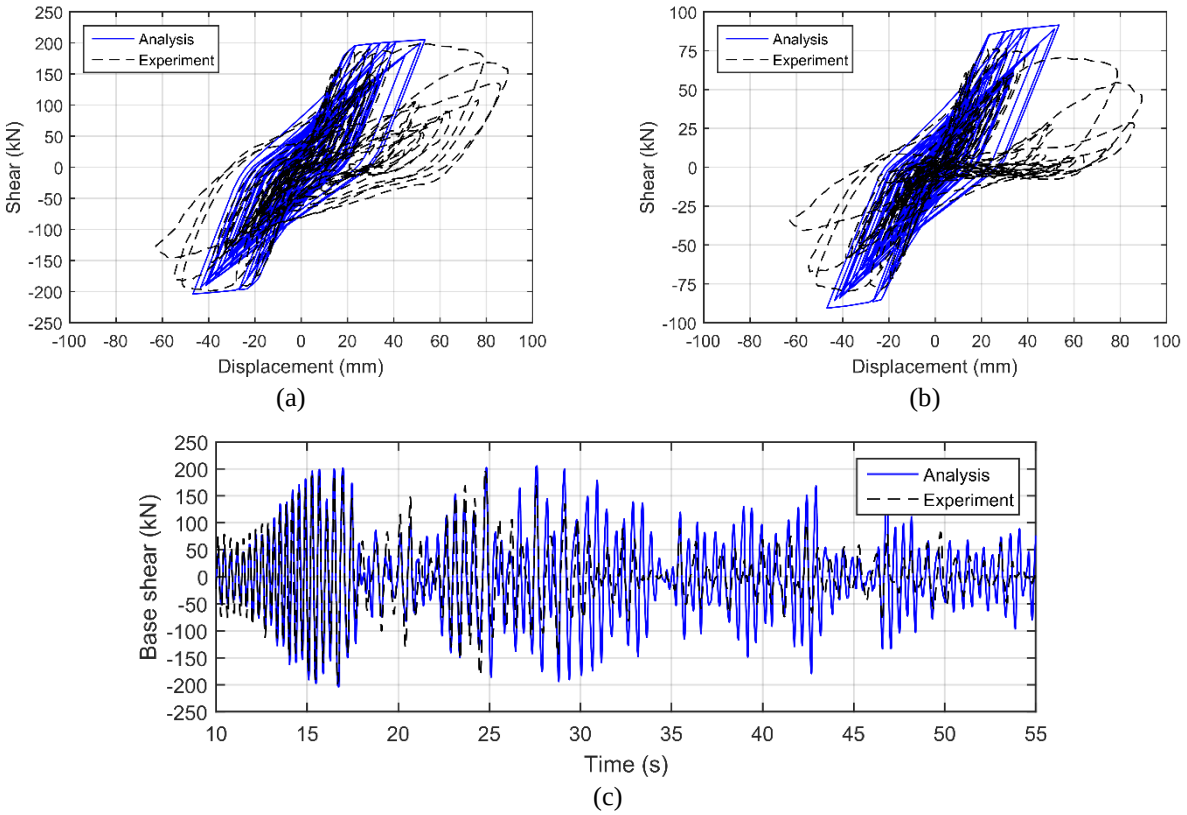

Figure 18: Comparison between the analytically predicted response without considering shear failure and the experimental test in terms of (a) base shear against lateral displacement of the first storey of the frame, (b) shear force against lateral displacement of the middle column and (c) base shear history.

Figure 16c demonstrates the cumulative energy dissipation throughout the shake-table test. Overall, it is predicted very well, albeit maintaining a small underestimation of about 6 kNm since the very first cycles, wherein limited energy is dissipated at the experimental test that is considered completely elastic behaviour by the analytical model. At the end of the test, there is a 15% difference between the two values (Table 1). Figure 16d shows the local V - γ relations at the top and bottom segments of the mid-column. Despite the fact that the shear force is equal in all segments, the local shear deformations at the top are way larger than the others, as expected due to shear failure, reaching values of almost 0.10. Simultaneously, the bottom segment also reaches significant deformations of up to 0.03, due to shear-flexure interaction inside the plastic hinge length. However, the bottom shear deformation is capped by its value at the onset of shear failure, in line with the finite element model formulation, whilst the top follows the prescribed post-peak descending branch.

Analytical results precluding the effect of shear failure are presented in Figure 18. The response is identical up to the onset of shear failure, deviating substantially after that, though. There is no strength degradation in the hysteretic response depicted in Figure 18a, b, which the experimental response exhibits, hence the strength and the energy dissipation are grossly overestimated. The strength overestimation can be much more clearly seen in Figure 18c, particularly after about 27 s. Simultaneously, the system is rendered much stiffer, resulting in far lower lateral displacements of the R/C frame. This can be more clearly observed in Figure 18a, with the frame's lateral displacements being significantly underestimated, barely exceeding 50 mm, while the experimental response reaches 90 mm. This is in line with comments made by the research team that conducted the experiments, who also investigated analytically identical, non-degrading frames [45], and underlines the significance of

appropriately modelling the post-peak response in shear deficient R/C sub-assemblages.

5. CONCLUSIONS

The post-peak response of shear and flexure-shear critical R/C elements as well as the localisation of post-peak shear deformations have to be appropriately captured, in order to correctly assess the degrading response of sub-standard structures to earthquake-induced actions, especially when it comes to predicting the initiation and cascade of progressive collapse. Concentrated inelasticity models, albeit computationally effective, are subject to limitations regarding their ability to predict inelastic response, with regard to capturing the gradual spread of inelasticity as well as the actual distribution of deformations and damage along structural elements. Distributed inelasticity models, on the other hand, have been found to suffer from numerical localisation issues in the softening regime, inherent to their numerical formulation, rendering their global and local predictions dependent on the chosen finite element mesh or numerical integration scheme, thus non-objective. Regularisation techniques have been proposed, providing realistic and physically meaningful solutions in terms of local deformations spread and magnitude after the onset of flexural failure, but no past study addresses the regularisation of softening post-peak response in the case of shear failure.

A beam-column finite element model for shear-deficient R/C elements has been put forward herein. It is a computationally efficient, flexibility-based, distributed-inelasticity, phenomenological model predicting the hysteretic non-linear response of shear and flexure-shear critical R/C members up to the onset of axial failure. Being based on local deformation quantities in lieu of inter-storey displacements, it can account in an unbiased way for the interaction of inelastic flexural and shear deformations, including the gradual decrease of an element's shear resistance, and more reliably predict the location and extent of shear deformations subsequent to shear failure, avoiding shortcomings of previous models. The analytical model formulation, displacement sub-components, element stiffness derivation in pre- and post-peak domain, application of post-peak strength degradation and shear failure localisation and the sub-models' interaction in unloading and reloading, have been discussed in detail.

Subsequently, the analytical model was verified against experimental quasi-static cyclic tests of double-curvature shear and flexure-shear critical columns as well as a shake-table test of a two-bay one-storey R/C frame. It was found to provide very good estimations of the response in all cases; in the dynamic shake-table test it was found to result in very good agreement, besides the residual lateral drift that was not observed in the analysis. More importantly, it was shown to fare satisfactorily not only in terms of total lateral displacement, but also in terms of individual displacement components. Achieving such level of agreement with individual experimental displacement components is no simple feat for a finite element model. For the purpose of comparison, objective accuracy measures quantifying the performance of the analytical model with regard to the experimental response were proposed and used, so that the results can be meaningfully compared with future analytical predictions.

The accuracy, versatility and simplicity of this beam-column finite element model make it a valuable tool in seismic analysis of complex R/C buildings with shear deficient structural elements.

6. ACKNOWLEDGEMENTS

This research study was conducted as part of the doctoral degree of the first author funded by City, University of London and the A. G. Leventis Foundation.

7. REFERENCES

1. Zimos DK, Mergos PE, Kappos AJ. Modelling of R/C members accounting for shear failure localisation: Hysteretic shear model. *Earthquake Engineering & Structural Dynamics* 2017.
2. Calabrese A, Almeida JP, Pinho R. Numerical issues in distributed inelasticity modeling of RC frame elements for seismic analysis," *Journal of Earthquake Engineering* 2010, **14**(S1): 38–68. DOI: 10.1080/13632461003651869
3. Giberson M. The response of nonlinear multi-story structures subjected to earthquake excitation. *PhD Thesis* 1967, California Institute of Technology.
4. Roufaiel MSL, Meyer C. Analytical Modeling of Hysteretic Behavior of R/C Frames**.** *Journal of Structural Engineering* 1987, **113**(3): 429-444. DOI: 10.1061/(ASCE)0733-9445(1987)113:3(429)
5. Thom C. The effects of inelastic shear on the seismic response of structures. *PhD Thesis* 1983, University of Auckland.
6. Ricles J, Yang Y, Priestley M. Modeling nonductile R/C columns for seismic analysis of bridges**.** *Journal of Structural Engineering* 1998, **124**(4): 415–425. DOI: 10.1061/(ASCE)0733-9445(1998)124:4(415)
7. Pincheira JA, Dotiwala FS, D'Souza JT. Seismic analysis of older reinforced concrete columns. *Earthquake Spectra* 1999, **15**(2): 245–272. DOI: 10.1193/1.1586040
8. Lee DH, Elnashai AS. Seismic analysis of RC bridge columns with flexure-shear interaction**.** *Journal of Structural Engineering* 2001, **127**(5): 546–553. DOI: 10.1061/(ASCE)0733-9445(2001)127:5(546)
9. Elwood KJ. Modelling failures in existing reinforced concrete columns. *Canadian Journal of Civil Engineering* 2004, **31**(5): 846–859. DOI: 10.1139/L04-040
10. Sezen H. Shear deformation model for reinforced concrete columns. *Structural Engineering and Mechanics* 2008, **28**(1): 39–52.
11. Sezen H, Chowdhury T. Hysteretic model for reinforced concrete columns including the effect of shear and axial load failure. *Journal of Structural Engineering* 2009, 135(2): 139–146. DOI: 10.1061/(ASCE)0733-9445(2009)135:2(139)
12. Soleimani D, Popov EP, Bertero VV. Nonlinear beam model for R/C frame analysis. *7th conference on electronic computation* 1979.
13. Valles R, Reinhorn A, Kunnath S, Li C, Madan A. IDARC2D, version 4.0: A computer program for the inelastic damage analysis of buildings. *Technical Report NCEER-96-0010* 1996.
14. Mergos PE, Kappos AJ. A gradual spread inelasticity model for R/C beam–columns, accounting for flexure, shear and anchorage slip. *Engineering Structures* 2012, **44**: 94–106. DOI: 10.1016/j.engstruct.2012.05.035
15. Hellesland J, Scordelis AC. Analysis of R.C. bridge columns under imposed deformations**.** *IABSE Colloquium on advanced mechanics of reinforced concrete* 1981: 545–559.
16. Spacone E, Filippou FC, Taucer FF. Fibre beam-column model for non-linear analysis of R/C frames: Part I. Formulation**.** *Earthquake Engineering & Structural Dynamics* 1996, **25**(7): 711–725. DOI: 10.1002/(SICI)1096-9845(199607)25:7<711::AID-EQE576>3.0.CO;2-9
17. Filippou FC, Ambrisi AD, Issa A. Nonlinear static and dynamic analysis of reinforced concrete subassemblages. *Report No. UCB/EERC 92–08* 1992.
18. Mullapudi TR, Ayoub A. Modeling of the seismic behavior of shear-critical reinforced concrete columns**.** *Engineering Structures* 2010, **32**(11): 3601–3615. DOI: 10.1016/j.engstruct.2010.08.004
19. Saritas A, Filippou FC. Inelastic axial-flexure–shear coupling in a mixed formulation beam finite element**.** *International Journal of Non-Linear Mechanics* 2009, **44**(8): 913–922. DOI: 10.1016/j.ijnonlinmec.2009.06.007
20. Ranzo G, Petrangeli M. A fibre finite beam element with section shear modelling for seismic analysis of RC structures. *Journal of Earthquake Engineering* 1998, **2**(3): 443–473. DOI: 10.1080/13632469809350330
21. Petrangeli M, Pinto P, Ciampi V. A fibre element for cyclic bending and shear. I: Theory**.** *Journal of Engineering Mechanics* 1999, **125**(9): 994–1001. DOI: 10.1061/(ASCE)0733-9399(1999)125:9(994)
22. Martinelli L. Modeling shear-flexure interaction in reinforced concrete elements subjected to cyclic lateral loading. *ACI Structural Journal* 2008, **105**(6): 675–684.
23. Ceresa P, Petrini L, Pinho R. Flexure-shear fiber beam-column elements for modeling frame structures under seismic loading — State of the art. *Journal of Earthquake Engineering* 2007, **11**(S1): 46–88. DOI: 10.1080/13632460701280237
24. Ceresa P, Petrini L, Pinho R, Sousa R. A fibre flexure–shear model for seismic analysis of RC- framed structures**.** *Earthquake Engineering & Structural Dynamics* 2009, **38**(5): 565–586. DOI: 10.1002/eqe.894
25. Filippou FC, Gregori JN, Sosa PM, Fern M. A. A 3D numerical model for reinforced and prestressed concrete elements subjected to combined axial , bending , shear and torsion loading. *Engineering Structures* 2007, **29**(12): 3404–3419. DOI: 10.1016/j.engstruct.2007.09.001
26. Bairan JM, Mari AR. Multiaxial-coupled analysis of RC cross-sections subjected to combined forces**.** *Engineering Structures* 2007, **29**(8): 1722–1738. DOI: 10.1016/j.engstruct.2006.09.007
27. Mohr S, Bairan JM, Mari AR. A frame element model for the analysis of reinforced concrete structures under shear and bending. *Engineering Structures* 2010, **32**(12): 3936–3954. DOI: 10.1016/j.engstruct.2010.09.005
28. Mazars J, Kotronis P, Ragueneau F, Casaux G. Using multifiber beams to account for shear and torsion. Applications to concrete structural elements**.** *Computer Methods in Applied Mechanics and Engineering* 2006, **195**(52): 7264–7281. DOI: 10.1016/j.cma.2005.05.053
29. Guner S, Vecchio FJ. Simplified method for nonlinear dynamic analysis of shear-critical frames**.** *ACI Structural Journal* 2012, **109**(5): 727–738.
30. Marini A, Spacone E. Analysis of reinforced concrete elements including shear effects**.** *ACI Structural Journal* 2006, **103**(5): 645–655.
31. Scott MH, Fenves GL. Plastic hinge integration methods for force-based beam – Column elements**.** *Journal of Structural Engineering* 2006, **132**(2): 244–252. DOI: 10.1061/(ASCE)0733-9445(2006)132:2(244)
32. Coleman J, Spacone E. Localization issues in force-based frame elements**,"** *Journal of Structural Engineering* 2001, **127**(11): 1257–1265. DOI: 10.1061/(ASCE)0733-9445(2001)127:11(1257)
33. Mergos PE, Kappos AJ. Analytical study on the influence of distributed beam vertical loading on seismic response of frame

structures. *Earthquakes and Structures* 2013, **5**(2): 239–259. DOI: 10.12989/eas.2013.5.2.239
34. Sivaselvan M, Reinhorn A. Hysteretic models for cyclic behavior of deteriorating inelastic structures. *Technical Report MCEER-99-0018* 1999.
35. Saatcioglu M, Alsiwat JM, Ozcebe G. Hysteretic behavior of anchorage slip in R/C members. *Journal of Structural Engineering* 1992, **118**(9): 2439–2458. DOI: 10.1061/(ASCE)0733-9445(1992)118:9(2439)
36. Mergos PE, Kappos AJ. Damage analysis of reinforced concrete structures with substandard detailing**.** *Computational Methods in Earthquake Engineering* 2013, **30**: 149–176. DOI: 10.1007/978-94-007-6573-3_8
37. Reinhorn A, Roh H, Sivaselvan M, Kunnath SK, Valles R, Madan A, Li C, Lobo R, Park YJ. IDARC2D version 7.0: A program for the inelastic damage analysis of structures. *Technical Report MCEER-09-0006* 2009.
38. Ozcebe G, Saatcioglu M. Hysteretic shear model for reinforced concrete members. *Journal of Structural Engineering* 1989, **115**(1): 132–148. DOI: 10.1061/(ASCE)0733-9445(1989)115:1(132)
39. LeBorgne MR, Ghannoum WM. Analytical element for simulating lateral-strength degradation in reinforced concrete columns and other frame members. *Journal of Structural Engineering* 2014, **140**(7): 04014038. DOI: 10.1061/(ASCE)ST.1943-541X.0000925
40. Huang X, Kwon OS. Numerical models of RC elements and their impacts on seismic performance assessment. *Earthquake Engineering & Structural Dynamics* 2015, **44**(2): 283–298. DOI: 10.1002/eqe.2471
41. Sezen H, Moehle JP. Seismic tests of concrete columns with light transverse reinforcement. *ACI Structural Journal* 2006, **103**(6): 842–849.
42. Lejano BA, Adachi H, Shirai N, Nakanishi M. Deformation characteristics of RC columns subjected to high and fluctuating axial load. *Journal of Structural and Construction Engineering (Transactions of AIJ)* 1995, **60**(467): 93–104. DOI: 10.3130/aijs.60.93_1
43. Aboutaha RS, Jirsa JO, Kreger ME, Engelhardt MD. Rehabilitation of shear critical concrete columns by use of rectangular steel jackets. *ACI Structural Journal* 1999, 96(1): 68-78.
44. Elwood KJ, Moehle JP. Dynamic shear and axial-load failure of reinforced concrete columns**.** *Journal of Structural Engineering* 2008, **134(**7): 1189–1198. DOI: 10.1061/(ASCE)0733-9445(2008)134:7(1189)
45. Elwood KJ, Moehle JP. Dynamic collapse analysis for a reinforced concrete frame sustaining shear and axial failures**.** *Earthquake Engineering & Structural Dynamics* 2008, **37**(7): 991–1012. DOI: 10.1002/eqe.787